Journal Name

Dynamic Article Links ►

Cite this: DOI: 10.1039/c0xx00000x

www.rsc.org/xxxxxx

ARTICLE TYPE

Post-metalation of porous aromatic frameworks for highly efficient carbon capture from CO_2+N_2 and CH_4+N_2 mixtures

Heping Ma[a], Hao Ren[a], Xiaoqin Zou[a], Shuang Meng[a], Fuxing Sun[a], and Guangshan Zhu[ab]*

Received (in XXX, XXX) Xth XXXXXXXXX 20XX, Accepted Xth XXXXXXXXX 20XX
DOI: 10.1039/b000000x

The development of microporous materials for carbon capture, especially for carbon dioxide and methane, is a rapid-growing field based on increasing demand for clean energy and pressing environmental concerns of global warming affected by greenhouse gases. To achieve this goal of developing carbon selective porous materials, a new porous aromatic framework featuring carboxyl-decorated pores, PAF-26-COOH, has been synthesized successfully. The modification of PAF-26 materials with representative light metals is exemplified by Li, Na, K and Mg via post-metalation approach. The obtained PAF-26 products exhibit moderate surface area and controllable pore size at atom level. Gas sorption of CO_2, CH_4 and N_2 is carried out on as-prepared PAF-26 samples at mild temperatures (273 K and 298 K). It is found that the PAF-26 materials show high adsorption capacity for CO_2 and CH_4 and low ability toward N_2. Particularly, as-synthesized PAF-26 compounds exhibit remarkably high isosteric heats of adsorption toward CO_2 and CH_4, indicating high affinity for CO_2 and CH_4 gases. The gas selectivity for CO_2/N_2 and CH_4/N_2 mixtures is predicted by IAST model. High selectivity of 80 for CO_2 over N_2 is obtained for PAF-26-COOMg. In addition, high selectivity values of CH_4 over N_2 are observed. The high performance including high storage capacity and selectivity makes PAF-26 materials promising in carbon capture or sequestration.

Introduction:

One of the most pressing environment concerns of our age is the escalating level of atmospheric greenhouse gas (mainly CO_2), which is deemed as a significant contribution to global warming.[1] Flue gas emissions of power plants are responsible for roughly 30% of total CO_2 emissions. Nitrogen is a main component (> 70%) of flue gas whereas the major impurity is CO_2 (10-15%), thus it is required to separate of CO_2 from N_2.[2] Another energy-related separation involves the purification of CH_4 from natural gas, since natural gas is mainly composed of valuable methane, typically 80-95%, with N_2 and CO_2 impurities of 5-10% depending on different gas reservoirs. In addition, landfill gas and coal-bed gas are rapidly growing as complements for natural gas; however, it often contains unacceptable levels of N_2 contaminants. The separation of methane from nitrogen is essential for natural gas upgrading and landfill and coal-bed gases purification to improve its purity in order to meet the specific criteria. Thus, carbon capture and separation (CCS) is therefore highly demanded. Consequently, sorption-based techniques or processes (usually involving solid adsorbents) have been innovated for CCS, which plays a leading role among versatile approaches.[3] Therefore, intensive efforts have been made to investigate the use of solid adsorbents for carbon capture and storage. In the library of solid adsorbents, porous materials such as zeolites,[4] carbons,[5] mesoporous silica-supported amines,[6] and metal organic frameworks,[7] have exhibited their good performances for practical CCS implementation. Very recently, porous organic frameworks (POFs) have also been proposed as new porous adsorbents for carbon capture and storage.[8] POFs composed of light elements *via* robust covalent bonds, are emerging as a new family of porous architectures and attracting increasing attention thanks to their high stability, tunable building blocks, controlled pore connectivity, and featuring opportunities for further functionality.[9] To achieve the goal of high-performance gas capture and storage with enhanced capacity and selectivity using POF materials, rational modification of POF skeletons with variable functionalities is deemed to be an appropriate approach.[10] Zhou's group have reported sulfonate-grafted and polyamine-tethered porous polymer networks exhibit exceptionally high binding affinity and large selectivity for CO_2.[10a, 11h] Generally, gas storage in POFs is greatly relevant with the pore size and the polarity of pore surface. The controlling of pore property in POFs is almost by changing the functional group in the organic monomer. Tailoring electrostatic interaction on the pore surface at the atom level such as introducing different metal ion in the porous skeleton may be a liable fashion to fine-control the pore property. The incorporation of metal ion can introduce point charges into the host material framework. By changing the atomic numbers of incorporated metal, we can tune the electrostatic charge-quadrupole and charge-induced dipole interactions with gas molecules on pore

surface.[11] In this study, we report the design and synthesis of a carboxyl-functionalized porous aromatic framework (PAF) material with permanent porosity, PAF-26-COOH, and a series of light metalized derivatives, referred as PAF-26-COOM (M = Li, Na, K, Mg) (Scheme 1). The resulting PAF-26-COOM materials are examined for CH_4, CO_2 and N_2 sorption. Further, the effects of pore size, surface area and isosteric heat of adsorption on a group of PAF-26-COOM materials will be investigated in details. Besides, the adsorption capacity and selectivity of these metalized PAF materials for CO_2 and CH_4 in CO_2/N_2 and CH_4/N_2 binary mixtures are estimated.

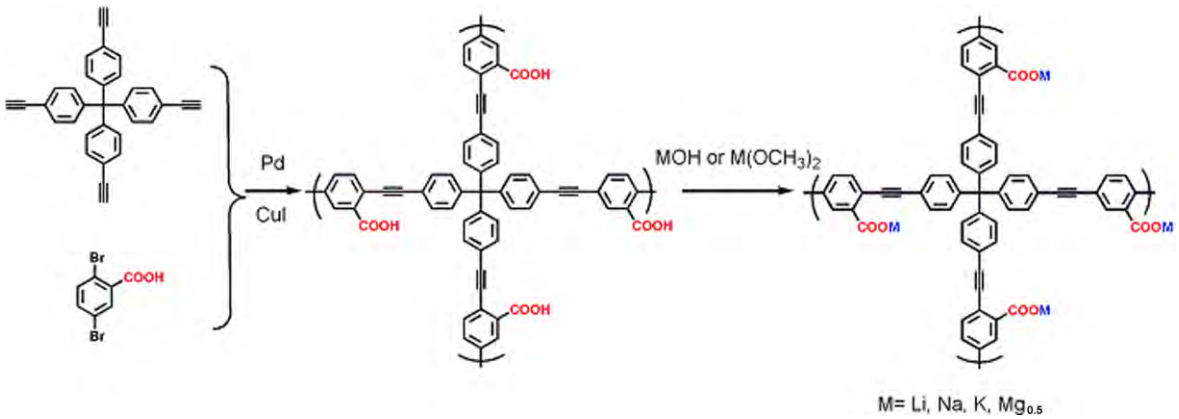

Scheme 1 Schematic representation for the synthesis of PAF-26-COOH and PAF-26-COOM using tetrakis(4-ethynylphenyl)methane and 2,5-dibromobenzoic acid

Experimental Section

1.1. Chemicals

The chemicals were purchased from Aldrich, Alfa-Aesar, and Aladdin-reagent, and used as received unless it was noted. *N,N*-dimethylformamide (DMF) and triethylamine (Et_3N) were dehydrated with CaH_2. Magnesium methoxide solution (7-8%) in methanol was purchased from Alfa-Aesar. Tetrakis(4-ethynylphenyl)methane was prepared according to the previously reported method.[9f] 2,5-dibromo-benzoic acid was purchased from Aladdin-reagent.

1.2. Synthesis of PAF-26-COOH

PAF-26-COOH was synthesized *via* palladium-catalyzed Sonogashira-Hagihara cross-coupling reaction. Typically, tetrakis(4-ethynylphenyl)methane (250 mg, 0.6 mmol), 2,5-dibromobenzoic acid (335 mg, 1.2 mmol), tetrakis(triphenphosphine)palladium (45 mg), and copper iodide (15 mg) were dissolved in the mixture of DMF (15 mL) and Et_3N (15 mL) in a 50 mL two-neck flask. After degassing *via* three freeze-pump-thaw cycles, the mixture was stirred at 100 °C for 36 h under N_2 atmosphere. After cooling down to room temperature, the resulting PAF-26-COOH was collected by filtration, followed by consecutive washing with chloroform (10 mL), methanol (10 mL), and water (10 mL) to remove the unreacted monomers and catalysts. As-prepared PAF-26-COOH was further purified *via* Soxhlet extraction with methanol for 48 h. After drying at 90 °C in vacuum overnight, PAF-26-COOH was obtained in the form of yellow powder (352 mg, 89% yield).

1.3. Post-metalation of PAF-26-COOH

1.3.1. Synthesis of PAF-26-COOLi, PAF-26-COONa and PAF-26-COOK

10 mg LiOH was added to a mixture of PAF-26-COOH (100 mg) in CH_3OH/H_2O (10 mL/10 mL). The resulting mixture was stirred at room temperature for 1 d. Subsequently, the solid was collected by filtration, washed with water several times to completely remove LiOH residues, and dried to produce PAF-26-COOLi yellow powder (95 mg).

The PAF-26-COONa and PAF-26-COOK were prepared in the same procedure by using NaOH and KOH as alkaline sources, respectively.

1.3.2. Synthesis of PAF-26-COOMg

Magnesium methoxide (7-8% in methanol solution) is considered as the suitable alkaline source to overcome the poor solubility of $Mg(OH)_2$ in CH_3OH or water. Typically, 210 μL magnesium methoxide solution was added to a mixture of PAF-26-COOH (100 mg) and anhydrous methanol (15 mL) in a dry 50 mL flask. The resulting mixture was then stirred in a dry atmosphere at room temperature for 12 h. Then, the solid was collected by filtration, washed with anhydrous methanol several times. After drying at 90 °C in vacuum for 10 h, PAF-26-COOMg yellow power (92 mg) was obtained.

2. Characterizations

FTIR spectra were obtained using an IFS 66V/S Fourier transform infrared spectrometer. Thermogravimetric analysis was implemented using a Netzch Sta 449c thermal analyzer system at a heat rate of 10 °C min^{-1} under air. Scanning electron microscopy (SEM) imaging was performed on JEOS JSM 6700. X-ray diffraction (XRD) measurements were carried out on Riguku D/MAX2550 diffractometer with Cu-Kα radiation (λ = 1.5418 Å) running at a voltage of 50 kV and a current of 200 mA. Solid-state ^{13}C CP/MAS NMR measurement was carried out on a Bruker Avance III model 400 MHz NMR spectrometer at a MAS rate of 5 kHz. The metal content in metalized porous frameworks was determined by inductively coupled plasma (ICP) spectroscopy (Perkin-Elmer ICP-OES Optima 3300DV). The typical procedure includes: (1) the digestion of samples (~15 mg) in 3:1 HCl/HNO_3 10 mL solution and heated at 120 °C in a 15 mL autoclave for 12 h; (2) after cooling down to room temperature, the solution was filtered and transferred to a 50 mL volumetric flask with distilled water.

3. Low-Pressure Gas Adsorption Measurements

The gas sorption isotherms were measured on a Quantachrome Autosorb iQ2 analyzer. Prior to the measurements, the samples were degassed at 120 °C for 24 h. N_2 sorption isotherms were recorded at 77 K, 273 K, and 298 K; CH_4 and CO_2 sorption measurements were performed at 273 K and 298 K, respectively. Ultra-high-purity grade (99.99%) N_2, CH_4, and CO_2 gases were used for all adsorption measurements. Liquid nitrogen bathes were utilized to control the temperature at 77 K. Ice-water and water bathes equipped with a temperature sensor were used to control the temperature at 273 K and 298 K.

Results and Discussion

Description of PAF-26-COOH and PAF-26-COOM:

To build a porous architecture, the secondary building blocks with tetrahedral geometry are employed to form 3-D porous organic frameworks *via* its co-condensation with linear building blocks. Additionally, the functional groups on the building blocks and their connection modes determine the physicochemical properties of organic frameworks. For this concept, PAF-26-COOH is prepared by the condensation of tetrakis(4-ethynylphenyl)methane as the tetrahedral node, and 2,5-dibromo-benzoic acid as the linear linker *via* Sonogashira-Hagihara cross-coupling reaction (Scheme 1).[12] Further, PAF-26-COOH bearing free carboxylic groups in the skeleton is post-modified with different light metals, and the corresponding products are designated as PAF-26-COOM. For better illustration of the connectivity and geometry about carbon atoms in PAF-26-COOH structure, this PAF material was characterized by solid-state ^{13}C cross-polarization magic-angle spinning (CP/MAS) NMR and Fourier transform infrared (FTIR) spectroscopy. Fig 1 shows the ^{13}C CP/MAS NMR spectrum of PAF-26-COOH solid sample. The NMR signal around 168 ppm is observed, which is assigned to the carbon atom in the carboxyl groups. This means that the

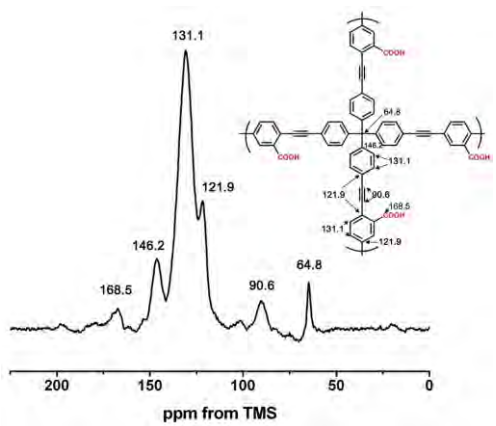

Fig. 1 ^{13}C CP/MAS NMR spectrum of PAF-26-COOH.

carboxyl groups remain intact, which makes further modification possible. A well-resolved peak is detected at 64.8 ppm associated with the quaternary carbon atom in the tetrakis(4-ethynylphenyl)methane, indicating that the tetrakis(4-ethynylphenyl)methane is the main component in the final PAF-26-COOH product.[13] A distinct NMR shift assigned to the benzene rings at 131.1 ppm appears, which indicates PAF-26-COOH framework is composed of highly conjugated phenyl groups.

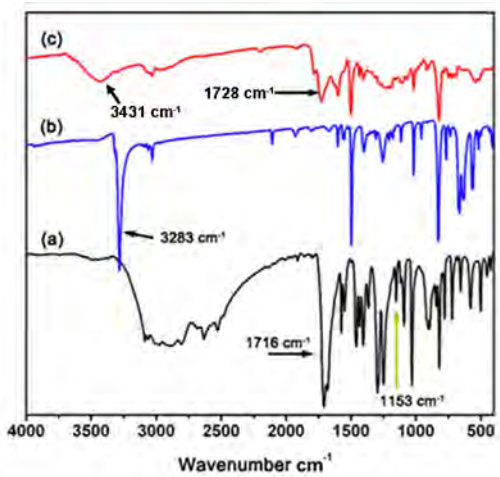

Fig. 2 FT-IR spectra of starting materials of 2,5-dibromobenzoic acid (a), tetrakis(4-ethynylphenyl)methane (b) and as-prepared PAF-26-COOH (c).

The PAF-26-COOH sample is further studied by FT-IR spectroscopy. The IR spectra of as-prepared PAF-26-COOH and their starting monomers are shown in Fig 2. The disappearance of peak at 3283 cm^{-1} associated with ≡C-H in the PAF-26-COOH product (Fig. 2c) provides direct evidence for the completed cross-coupling reaction. The IR band corresponding to the stretching vibrations of –COO group (1728 and 3431 cm^{-1}) in the PAF-26-COOH sample are similar to that of its monomer 2,5-dibromo-benzoic acid (Fig 2a), which means that -COO groups are kept unchanged during the reaction. The band related with C-Br vibration mode at 1153 cm^{-1} (Fig 2a) vanishes into the background, which gives distinct proof for the complete reaction between these two monomers (Fig 2c). The metalized derivatives PAF-26-COOM were also characterized by IR spectroscopy and their IR spectra were recorded in Fig. 3. Shoulder bands around 1683 cm^{-1}, 1683 cm^{-1}, 1681 $cm^{-1}$and 1685 cm^{-1} for PAF-26-COOLi, PAF-26-COONa, PAF-26-COOK and PAF-26-COOMg samples grow conjointly with the ones at 1722 cm^{-1}, 1721 cm^{-1}, 1720 cm^{-1}, 1724 cm^{-1}, respectively. These additional bands are assigned to the -COO groups linked with metal cations, which is not observed in the case of PAF-26-COOH. The metal loading in PAF-26-COOM was analyzed by inductively coupled plasma optical emission spectroscopy (ICP-OES). It is found that the protons in the carboxyl groups of PAF-26-COOH are almost stoichiometry substitution by metal ions (Table 1), affording corresponding PAF-26-COOLi, PAF-26-COONa, PAF-26-COOK and PAF-26-COOMg products. This high replacement of protons (about 85 %) confirms that nearly all the carboxyl groups in PAF-26-COOH framework are available for post-metallization, which is in agreement with the IR result. The isolated PAF-26-COOH and its corresponding derivative PAF-26-COOM powders are subjected to XRD and SEM characterizations. Based on the XRD study (Fig S1), all of them exist as amorphous polymers. Spherical aggregates with small particles in size of 3-5 μm are observed in SEM pictures (Fig S2). The thermal stability of PAF26s is studied by TGA (Fig S3). A distinct weight loss in a range of 300 – 400 °C is observed, which corresponds to the decomposition or collapse of the organic

skeleton.

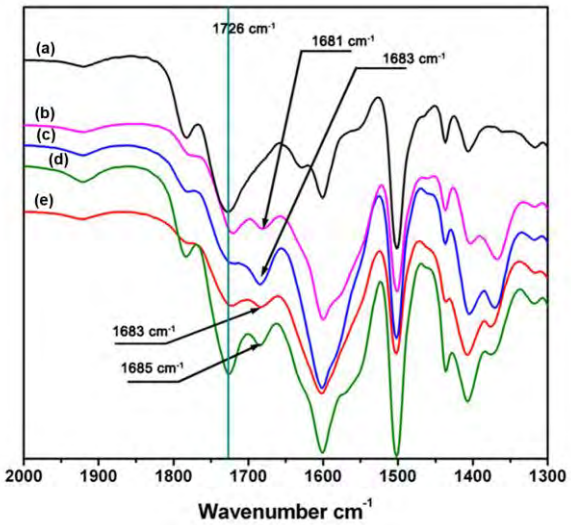

Fig. 3 FT-IR spectra of (a) PAF-26-COOH, (b) PAF-26-COOK, (c) PAF-26-COONa, (d) PAF-26-COOMg, (e) PAF-26-COOLi.

Porosity of PAF-26-COOH and PAF-26-COOM:

The porosity and pore structures of PAF-26 series were investigated by nitrogen sorption measurement at 77 K. As shown in Fig. 4, a sharp increase in gas uptake is observed at low pressure in the nitrogen adsorption–desorption isotherms of PAF-26-COOH and PAF-26-COOM, which confirm the existence of micropores in PAFs. A mild hysteretic shoulder in the desorption isotherms prove that materials also feature a small degree of mesoporosity. For clear illustration, a series of pore parameters derived from the nitrogen isotherms are listed in Table 1, including Brunauer-Emmett-Teller (BET) apparent surface area, pore size, total pore volume and micropore volume. The surface area of PAF-26-COOM is a bit lower than that of PAF-26-COOH (717 $m^2\ g^{-1}$ for PAF-26-COOH, 591 $m^2\ g^{-1}$ for PAF-26-COOLi, 483 $m^2\ g^{-1}$ for PAF-26-COONa, 430 $m^2\ g^{-1}$ for PAF-26-COOK and 572 $m^2\ g^{-1}$ for PAF-26-COOMg, respectively). The replacement of hydrogen atoms with metal ions leads to a decrease of surface area, which is consistent with an increase of atomic weights from Li to K.

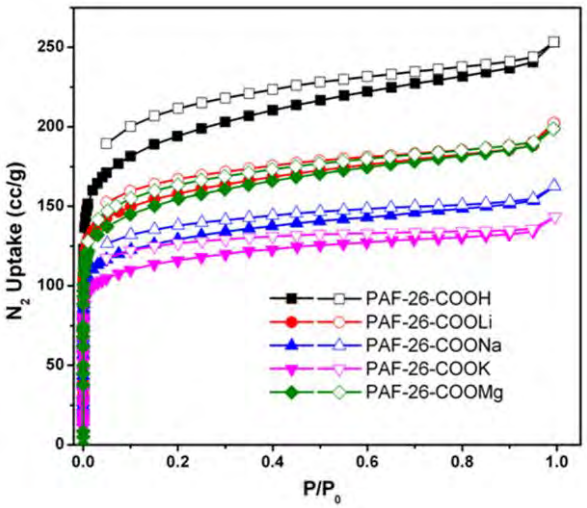

Fig. 4 N_2 adsorption-desorption isotherms measured at 77 K for PAF-26-COOH, PAF-26-COOLi, PAF-26-COONa, PAF-26-COOK and PAF-26-COOMg; adsorption branch in closed symbols, and desorption branch in open symbols.

Based on the non-local density functional theory (NLDFT), the pore size distribution (PSD) of PAF-26-COOH exhibits a dominant pore diameter of 0.52 nm, while the PSD of PAF-26-COOM exhibits dominant ones of about 0.52, 0.49, 0.48 and 0.57 nm, for PAF-26-COOLi, PAF-26-COONa, PAF-26-COOK and PAF-26-COOMg, respectively (Table 1 and Fig S4). The decreasing trend in the pore size for PAF-26-COOLi, PAF-26-COONa, PAF-26-COOK samples can be found in comparison to that of the parent sample of PAF-26-COOH, which can be explained by the increased ionic radius of Li^+ (90 pm), Na^+ (116 pm), and K^+ (152 pm). The pore size of PAF-26-COOMg is enlarged by exchanging proton with Mg^{2+} ions. This phenomenon can be interpreted with a first cleavage of hydrogen bonds between neighbor carboxylic groups, and further interacted with Mg^{2+} ion. Additionally, the pores in PAF-26-COOH and PAF-26-COOM are very uniform in microporous range, which is evidenced by the narrow pore size distribution (Fig. S4) and high micropore volume ratio (~ 90%, Table 1).

Table 1 Results from chemical analysis (ICP) and N_2-sorption measurements for PAF-26 samples including metal loadings, BET surface areas, pore volumes and their ratio, and pore sizes.

Samples	Theoretical metal loading (mmol g^{-1})	Actual metal loading (mmol g^{-1})[a]	BET SSA ($m^2\ g^{-1}$)[b]	V_{micro} ($cm^3\ g^{-1}$)	V_{total} ($cm^3\ g^{-1}$)[c]	V_{micro}/V_{total}	Pore size (nm)[d]
PAF-26-COOH		-	717	0.31	0.36	0.86	0.52
PAF-26-COOLi	3	2.45	591	0.24	0.28	0.86	0.52
PAF-26-COONa	3	2.6	483	0.20	0.23	0.87	0.49
PAF-26-COOK	3	2.4	430	0.19	0.20	0.95	0.48
PAF-26-COOMg	1.5	1.3	572	0.23	0.28	0.82	0.57

[a] Actual metal loading was analyzed by inductively coupled plasma optical emission spectroscopy (ICP-OES), [b] BET SSA was calculated in the partial pressure (p/p_0) range of 0.01-0.05 which gives the best linearity, [c] Total pore volume at relative pressure p/p_0= 0.99, [d] The pore size distribution calculated using the DFT method.

Gas Adsorption:

With the successful preparation of PAF-26 polymers with high porosity, fully available functional groups and a pore size around 0.5 nm, PAF-26-COOH and PAF-26-COOM materials are

evaluated for gas adsorption or capture. Typically, the adsorption properties of PAF materials for CO_2, CH_4, and N_2 were studied by gas adsorption measurements; of which CO_2 and CH_4 are two main carbon sources in the flue gas, natural gas or landfill gas. Fig. 5 displays CO_2 and CH_4 adsorption isotherms recorded at 273 K. There is a steep uptake at low relative pressures and followed by continuous sorption for CO_2 upon increasing the pressure (Fig. 5a). The CO_2 uptake for PAF-26-COOH sample is 52 cc g^{-1} at P = 101 kPa. With the substitution of protons by metal ions, improved sorption ability for CO_2 is attained (Fig. 5a). For better understanding the effect of different metal ions on the capture performance, the gas uptakes were normalized by the pore volume (V_{total}) to assess the sorption capacities between different adsorbents.[5f] The uptakes per effective V_{total} versus pressure for all PAF-26 materials toward CO_2 are plotted in Fig. 5b. A distinct enhancement is observed in the uptake per effective V_{total} after metallization with Li^+, Na^+, K^+ and Mg^{2+} if taking its proton form of PAF-26-COOH material as a reference (Fig. 5b). PAF-26-COOK can adsorb 572 mg CO_2 per cm^3, which is much higher than its parent PAF-26-COOH (286 mg cm^{-3}). This sheds light on improved adsorption affinity of PAF-26-COOM toward CO_2. In the same manner, methane adsorption was also carried out. Above 16 cc g^{-1} of methane are adsorbed in PAF-26 samples at 273 K and 101 kPa (Fig 5c). The uptakes per effective V_{total} in the dependence of pressure for PAF-26 series towards CH_4 are also calculated and shown in Fig. 5d. It can be found that CH_4 uptake per effective V_{total} increases from 34 mg cm^{-3} (PAF-26-COOH) to 46 mg cm^{-3} (PAF-26-COOLi, 35% increase), 54 mg cm^{-3} (PAF-26-COOMg, 59% increase), 56 mg cm^{-3} (PAF-26-COONa, 65% increase) and 60 mg cm^{-3} (PAF-26-COOK, 76% increase). Based on the observations above, it can be concluded that an introduction of metal active centers would greatly promote gas adsorption capacity (especially for CO_2 and CH_4) and discriminate the adsorption affinity toward specific gases. To probe the influence of water on CO_2 uptake, the pretreated PAF-26-COOMg samples was exposed to wet air (the average relative humidity is about 50%) for 3 days. As indicated in Fig. S8, the CO_2 uptake of the humidified sample represents a 38% drop relative to the outgassed network. This behavior is similar to –OH containing POPs under humid conditions, which also preferentially adsorb water molecules.[14] The cyclic CO_2 adsorption–desorption study is also carried out. As shown in Fig. S8, the CO_2 uptake of PAF-26-COOMg remains almost constant after exposure in air for more than 4 months, which implies that metalized PAFs are quite stable.

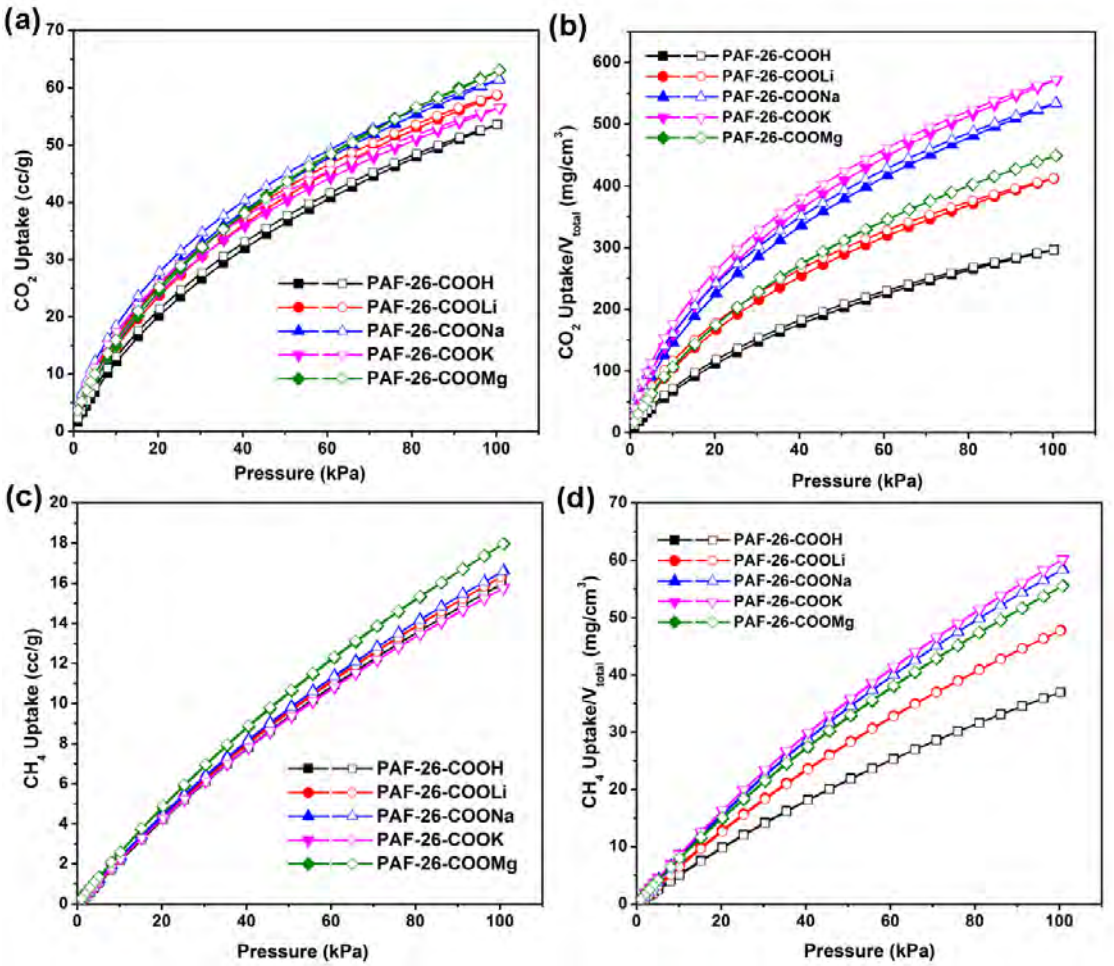

Fig. 5 Gas sorption isotherms of CO_2 (a), CO_2 uptakes per effective V_{total} (b), CH_4 (c), CH_4 uptakes per effective V_{total} (d) for PAF-26-COOH, PAF-26-COOLi, PAF-26-COONa, PAF-26-COOK and PAF-26-COOMg samples at 273 K and 101 kPa.

As we know, the isosteric heats of adsorption (Q_{st}) is another index to estimate the affinity of adsorbate to adsorbent,[15] which is helpful to understand the relationship between apparent sorption capacity and metal ions modified frameworks. Based on the adsorption isotherms at different temperatures (273 K and 298 K, Fig. S5-S6), the isosteric heats of adsorption of CO_2 and CH_4 can be determined for each material according to the Clausius-Clapeyron equation (the calculation is detailed in supporting information). As shown in Fig. 6a, the Q_{st} values of CO_2 for PAF-26-COOM have significantly increased compared with its counterpart of PAF-26-COOH. Typically, the CO_2 Q_{st} of PAF-26-COOH at low uptake is 28.1 kJ mol^{-1} (Fig. 6a and Table 2), while the CO_2 Q_{st} for PAF-26-COONa reaches 35.0 kJ mol^{-1} and notably high Q_{st} values for other metalized materials are also obtained (31.8 kJ mol^{-1}, 32.6 kJ mol^{-1} and 30.0 kJ mol^{-1} for PAF-26-COOLi, PAF-26-COOK and PAF-26-COOMg, respectively). The present data from adsorption measurements for iso-structural PAF-26 materials with exchanged metal ions shows a strong influence of metal sites on isosteric heats of adsorption. More interestingly, there is a decreasing trend in CO_2 Q_{st} values of 35.0, 32.6, 31.8, 30.0 kJ mol^{-1} with a sequence of PAF-26-COONa, PAF-26-COOK, PAF-26-COOLi and PAF-26-COOMg, which coincides with their corresponding basicity originated from compensated alkaline or earth alkaline ions (pK_b for PAF-26-COONa, PAF-26-COOK, PAF-26-COOLi, PAF-26-COOMg are 37.96, 36, 33.95, 15.08). Because there is less –COOH in the structural unit, the CO_2 Qst of PAF-26-COOH (28.1 kJ mol^{-1}) is lower than CMP-1-COOH (33 kJ mol^{-1}).[12c] Zhou's group reported a sulfonate-grafted PPN-SO_3H with CO_2 Qst value of 30.4 kJ mol^{-1}. After lithiation, the CO_2 Qst of PPN-6-SO_3Li reached 35.7 kJ mol^{-1}.[11h] In this case, after Na^+ metalized, the CO_2 Qst of PAF-26-COONa is up to 35 kJ mol^{-1}. which is comparable to the PPN-6-SO_3Li and Li doped MOFs.[11i] Nevertheless, these Q_{st} values of PAF-26-COOM are among many state-of-the-art excellent porous materials, which can be clearly seen in Table S2.

Parallel Q_{st} determination of CH_4 for PAF-26 materials was also carried out. The isosteric heats of adsorption for all measured materials are shown in Fig. 6b as a function of CH_4 gas uptake. As clearly seen in Fig. 6b and Table 2, the initial CH_4 Q_{st} values for PAF-26-COOLi, PAF-26-COOMg, PAF-26-COOK and PAF-26-COONa are 16.5, 21.5, 23.0, 24.0 kJ mol^{-1}, which are remarkably higher than that of PAF-26-COOH (14.3 kJ mol^{-1}). In general, a high isosteric heat of adsorption could lead to high gas storage at low pressures, which has already been exemplified by the adsorption measurements (Fig. 5). Notably, the high Q_{st} of PAF-26-COOM for CH_4 (16-24 kJ mol^{-1}) guarantees PAF-26 materials to be ranked in the top level of porous materials as can be seen from other outstanding porous materials, such as MIL-53 (18.0-19.0 kJ mol^{-1}),[16] HKUST-1 (16.6-20.7 kJ mol^{-1}),[17] MOF-5 (12.2 kJ mol^{-1}),[18] BILP-1 to BILP-7 (13-18.4 kJ mol^{-1}).[19] Furthermore, higher Q_{st} values for PAF-26-COOM provide evidence on stronger interaction between CH_4 molecules and PAF-26-COOM frameworks in contrast to PAF-26-COOH. Based on the results above, the possible reasons of strong interaction between PAF-26-COOM materials and CH_4 gas molecules can be explained as follows: on one hand, more charges on metal centers may facilitate to polarize the CH_4 molecule and cause stronger binding force. On the other hand, pore effect has to be regarded. Small pores would result in an overlap of the van der Waals forces of neighboring atoms, which gives rise to a strong interaction.[20] From the adsorption observations, one can conclude that PAF-26 materials with permanent small pores and high isosteric heats of adsorption have been synthesized.

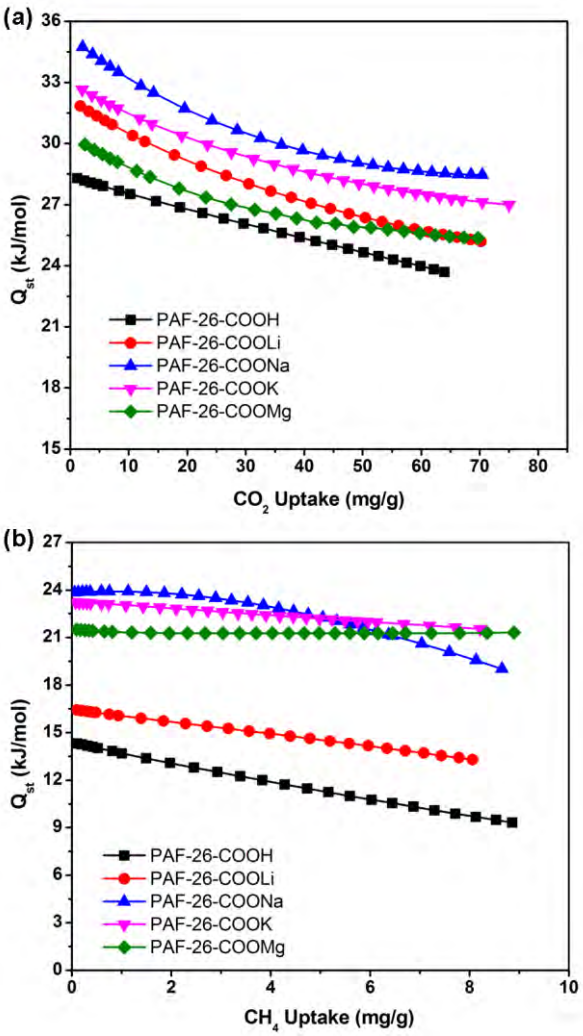

Fig. 6 The isosteric heats of adsorption for CO_2 (a) and CH_4 (b) of PAF-26-COOH, PAF-26-COOLi, PAF-26-COONa, PAF-26-COOK and PAF-26-COOMg in function of the gas uptake.

Gas Selectivity Studies:

The capture of CO_2 and CH_4 carbon resources is very important in energy conservation. For practical application, the separation of CO_2 from N_2 in flue gas is critical to reduce global greenhouse effect. The upgrading of landfill gas or coal-bed gas is demanded to extract CH_4 from N_2. High adsorption capacities of PAF-26 materials toward CO_2 and CH_4 are demonstrated, while very small uptake of (3 cc g^{-1}) is observed for N_2 at 101 kPa and 298 K (Fig. S7). Adsorption selectivity is another key parameter in pressure swing adsorption separation process with porous solid materials toward gases especially for carbon-rich CO_2 and CH_4, which are promising for carbon storage or capture in the future.

In this respect, the selectivity in the capture of CO_2 and CH_4 from CO_2/N_2, CH_4/N_2 gas mixtures is evaluated by ideal adsorption solution theory (IAST), which is well recognized and employed to predict gas mixture adsorption behaviors in porous materials.[21] As a result, selectivity studies of theoretical gas mixtures of CO_2/N_2, CH_4/N_2 were conducted by IAST model utilizing single-component isotherms.

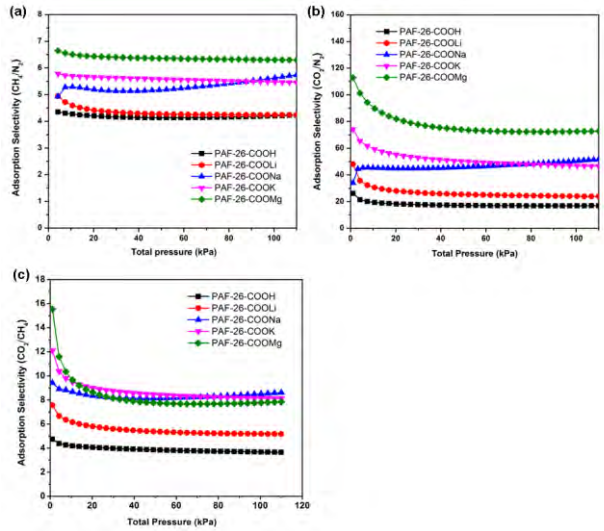

Fig. 7 IAST-predicted adsorption selectivity of CH_4/N_2 (a) and CO_2/N_2 (b) and CO_2/CH_4 (c) at 298 K and 110 kPa for PAF-26-COOH, PAF-26-COOLi, PAF-26-COONa, PAF-26-COOK and PAF-26-COOMg.

Based on single gas adsorption isotherms using IAST model, the selectivity of CH_4 over N_2 (1:1 in volume) for PAF-26 materials according to the experimental data is calculated and the results are shown in Fig. 7a. The resulting selectivity of CH_4 over N_2 with values of 4.2, 4.4, 5.5, 5.8 and 6.5 is obtained for PAF-26-COOH, PAF-26-COOLi, PAF-26-COONa, PAF-26-COOK and PAF-26-COOMg, respectively (Table 2). There is no loss in the CH_4 selectivity for these four samples in the whole test pressure range (0-110 kPa). As seen in Table 2, the selectivity of CH_4 over N_2 for PAF-26-COOM is higher than that of PAF-26-COOH (4.2), which provides a supporting evidence on the enhanced affinity to CH_4 after post metalation. The selectivity of all PAF-26 iso-structural materials (PAF-26-COOH and its light metalized derivatives, PAF-26-COOM) for CH_4 over N_2 surpasses the previously reported porous adsorbents, especially for PAF-26-COOMg with extraordinary high value of 6.5, ranking PAF-26-COOMg among the best porous adsorbents for separating CH_4 from N_2 (Table S2).

The calculated adsorption selectivity for 15% CO_2 and 85% N_2 mixtures in PAF-26 materials as a function of bulk pressure is presented in Fig. 7b. After post-metalation, the selectivity of PAF-26-COOM increases significantly in comparison with PAF-26-COOH. At 110 kPa, the selectivity of CO_2 over N_2 in PAF-26-COOH, PAF-26-COOLi, PAF-26-COONa and PAF-26-COOK is estimated to be 20, 24, 50 and 53 in the plateau (Fig. 7b). Exceptionally in the case of PAF-26-COOMg, the selectivity of CO_2 over N_2 reaches 80 under 110 kPa. The excellent CO_2 selectivity in PAF-26-COOMg may be explained by progressive CO_2 adsorption onto the active sites of high-valence magnesium under ambient pressure. The CO_2/N_2 selectivities of PAFs are lower than the N_2–phobic azo-COPs reported by Patel et al, which have the highest CO_2/N_2 selectivity (288) at 323K.[8f] The selectivity of CO_2 over CH_4 (1:1 in volume) is also examined as it involves the purification of CH_4 from natural gas. As shown in Fig. 7c, the CO_2/CH_4 selectivity of PAF-26-COOM are also increased in comparison to that of PAF-26-COOH. The selectivity of PAF-26-COONa (9) at 110 kPa is about two times more than that of PAF-26-COOH (4). Combined with adsorption and selectivity studies, one can be concluded that the carboxyl-functionalized and post-metalation PAF materials integrate two important characteristics of high sorption capacity and high selectivity. Such PAF materials may be an excellent candidate for carbon capture or storage.

Table 2 Isosteric heats of adsorption for CO_2 and CH_4, and selectivities of CO_2/N_2 and CH_4/N_2 for PAF-26 materials.

Samples	Q_{st} for CO_2	Q_{st} for CH_4	Selectivity for CO_2/N_2[a]	Selectivity for CO_2/CH_4[a]	Selectivity for CH_4/N_2[a]
PAF-26-COOH	28.1	14.3	20	4	4.2
PAF-26-COOLi	31.8	16.5	24	5.6	4.4
PAF-26-COONa	35.0	24.0	53	9	5.0
PAF-26-COOK	32.6	23.0	50	8.6	5.8
PAF-26-COOMg	30.0	21.5	73	8.4	6.5

[a] Selectivity was calculated by IAST at298 K and 110 kPa.

Conclusions

In summary, we have successfully designed and synthesized a carboxyl-functionalized PAF material, PAF-26-COOH. Post-metalation of PAF-26-COOH yields a series of PAF-26-COOM derivatives (M=Li, Na, K, Mg). The structure, morphology and porosity of PAF-26 products are comprehensively investigated by IR, NMR, XRD, SEM and N_2 adsorption measurements. Microporous PAF-26 materials with high surface area, high porosity and tunable pore size are achieved *via* post-metalation method. High adsorption capacities toward CO_2 and CH_4 are demonstrated with as-prepared PAF-26 materials, while very low uptake for N_2 is measured with the same samples. Additionally, an enhanced adsorption for CO_2 and CH_4 is observed for PAF-26-COOM in comparison to PAF-26-COOH, which indicates an introduction of light metal ions would improve the adsorption affinity to CO_2 and CH_4 gases. Further, PAF-26 materials exhibit very high isosteric heats of adsorption toward CO_2 and CH_4. Interestingly, the isosteric heats of adsorption for CO_2 follow in a sequence of PAF-26-COOMg<PAF-26-COOLi<PAF-26-COOK<PAF-26-COONa, which matches well with their corresponding basicities. The stronger interaction between CH_4 molecules and PAF-26-COOM is verified by their higher isosteric heats of adsorption, which is due to higher polarity of metal ions compared with proton and small-pore effect. The selective adsorption toward CO_2 and CH_4 over N_2 is studied and predicted selectivity is calculated by IAST model derived from their adsorption isotherms. All measured PAF-26 samples show high selectivity for CO_2 over N_2 with values of 20-80 and significantly high selectivity for CH_4 over N_2 with a highest value of 6.5. The combined merits of high sorption capacity and high selectivity offer PAF-26 as a potential stepping stone to porous materials for carbon capture and storage.

Acknowledgements

We are grateful to the financial support from National Basic Research Program of China (973 Program, grant nos.2012CB821700), Major International (Regional) Joint Research Project of NSFC (grant nos. 21120102034) NSFC (grant nos. 20831002, 21201074) and Australian Research Council Future Fellowship (FT100101059).

Notes and references

[a] *State Key Laboratory of Inorganic Synthesis & Preparative Chemistry, Jilin University, Changchun, 130012, China.*
Fax: (+86)431-8516-8331
E-mail: zhugs@jlu.edu.cn
[b] *Queensland Micro- and Nanotechnology Centre, Griffith University, Queensland, 4111, Australia.*

† Electronic Supplementary Information (ESI) available: [Additional figures of PAF-26-COOM (IR, XRD, SEM), pore size distribution, calculation of Qst, basicity and Ideal Adsorption Solution Theory (IAST) calculations]. See DOI: 10.1039/b000000x/

1 (a) S. A. Montzka, E. J. Dlugokencky, J. H. Butler, *Nature*,2011, **476**, 43; (b) G. Férey, C. Serre, T. Devic, G. Maurin, H. Jobic, P. L. Llewellyn, G. D. Weireld, A. Vimont, M. Daturi, J. S. Chang, *Chem. Soc. Rev.*, 2011, **40**, 550; (c) J. Liu, P. K. Thallapally, B. P. McGrail, D. R. Brown and J. Liu, *Chem. Soc. Rev.*, 2012, **41**, 2308;(d) G. Xiao , P. Xiao, S. Lee and P. A. Webley, *RSC Advances*, 2012, **2**, 5291.

2 (a) Y. S. Bae, R. Q. Snurr, *Angew. Chem. Int. Ed.*, 2011 **50** 11586; (b) D. M. D'Alessandro, B. Smit, J. R. Long, *Angew. Chem. Int. Ed*., 2010, **49***,* 6058; (c) Q. Wang, J. Luo, Z. Zhong, A. Borgna, *Energy. Environ. Sci.*, 2011, **4**, 42.

3 (a) P. Markewitz, W. Kuckshinrichs, W. Leitner, J. Linssen, P. Zapp, R. Bongartz, A. Schreiber, T. E. Müller, *Energy Environ. Sci.*, 2012, **5**, 7281; (b) L. S. Fan, L. Zeng, W. Wang, S. Luo, *Energy Environ. Sci.*, 2012, **5**, 7254.

4 (a) P. Y. Li, F. H. Tezel, *Microporous Mesoporous Mater*., 2007, **98**, 94; (b) S. Cavenati, C. A. Grande, A. E. Rodrigues, *J. Chem. Eng. Data.,* 2004, **49***,* 1095; (c) J. M. Leyssale, G. K. Papadopoulos, D. N. Theodorou, *J. Phys. Chem. B*., 2006, **110**, 22742; (d) L. Grajciar, J. Čejka, A. Zukal, Otero Areán, C. T. Palomino, G. P. Nachtigall, *ChemSusChem*, 2012, **5**, 2011.

5 (a) S. Cavenati, C. A. Grande, A. E. Rodrigues, *Sep. Sci. Technol.*, 2005, **40**, 2721; (b) R. Babarao, Z. Q.Hu, J. W. Jiang, S. Chempath, S. I. Sandler, *Langmuir*, 2007, **23**, 659; (c) M. B. Kim, Y. S. Bae, D. K. Choi, C. H. Lee, *Ind. Eng. Chem. Res.*, 2006, **45**, 5050; (d) V. Goetz, O. Pupier, A. Guillot, *Adsorption*, 2006, **12**, 55; (e) Z. Liu, C. A. Grande, P. Li, J. Yu, A. E. Rodrigues, *Sep. Sci. Technol.*, 2011, **46**, 434; (f) C. Pevida, M. G. Plaza, B. Arias, J. Fermoso, F. Rubiera, J. J. Pis, *Appl. Surf. Sci.* 2008, **254**, 7165.

6 (a) P. J. E. Harlick, A. Sayari, *Ind. Eng. Chem. Res.*, 2007, **46**, 446; (b) R. Serna-Guerrero, Y. Belmabkhout, A. Sayari, *Adsorption*, 2010, **16**, 567; (c) Y. Kuwahara, D. Y. Kang, J. R. Copeland, N. A. Brunelli, S. A. Didas, P. Bollini, C. Sievers, T. Kamegawa, H. Yamashita, C. W. Jones, *J. Am. Chem. Soc.* 2012, **134**, 10757; (d) S. A. Didas, A. R. Kulkarni, D. S. Sholl, C. W. Jones, *ChemSusChem*, 2012, **5**, 2058; (e) W. Chaikittislip, R. Khunsupat, T. T. Chen, C. W. Jones, *Ind. Eng. Chem. Res.* 2011, **50**, 14203; (f) S. Choi, M. L. Gray, C. W. Jones, *ChemSusChem*., 2011, **4**, 628; (g) W. Li, S. Choi, J. H. Drese, M. Hornbostel, G. Krishnan, P.M. Eisenberger, C. W. Jones, *ChemSusChem.* 2010**,** **3**, 899; (h) J. H. Drese, S. Choi, R. Lively, W. J. Koros, D. J. Fauth, M. L. Gray, C. W. Jones, *Adv. Funct. Mater. 2009*, **19**, 3821; (i) Y. Kuwahara, D. Y. Kang, J. R., Copeland, P. Bollini, C. Sievers, T. Kamegawa, H. Yamashita, C. W. Jones, *Chem. Eur. J.*, 2012, **18**, 16649.

7 (a) R. E. Morris, P. S. Wheatley, *Angew. Chem. Int. Ed.*, 2008, **47**, 4966; (b) T. M. McDonald, W. R. Lee, J. A. Mason, B. M. Wiers, C. S. Hong, J. R. Long, *J. Am. Chem. Soc.*, 2012, **134**, 7056; (c) J. R . Li, W. Lu, H. C. Zhou, *Chem. Soc. Rev*., 2012, **41**, 7761; (d) S. Choi, J. H. Drese, C. W. Jones, *ChemSusChem*, 2009, **2**, 796; (e) K. Sumida, D. L. Rogow, J. A. Mason, T. M. McDonald, E. D. Bloch, Z. R. Herm, T. H. Bae, J. R. Long. *Chem. Rev.*, 2012, **112**, 724; (f) R. Luebke, J. F. Eubank, A. J. Cairns, Y. Belmabkhout, L. Wojtas, M. Eddaoudi, *Chem. Commun.*, 2012, **48**, 1455.

8 (a) P. Pandey, A. P. Katsoulidis, I. Eryazici, Y. Wu, M. G. Kanatzidis, S. T. Nguyen, *Chem. Mater.*, 2010, **22**, 4974; (b) R. Dawson, E. Stöckel, J. R. Holst, D. J. Adams, A. I. Cooper, *Energy. Environ. Sci.*, 2011, **4**, 4239; (c) T. C. Drage, C. E. Snape L. A. Stevens, J. Wood, J. Wang, A. I. Cooper, R. Dawson, X. Guo, C. Satterley, R. Irons, *J. Mater. Chem.,* 2012, **22**, 2815; (d) Q. Chen, M. Luo, P. Hammershoj, D. Zhou, Y. Han, B. W. Laursen, C. G. Yan, B. H. Han, *J. Am. Chem. Soc.*, 2012, **134**, 6084; (e) Y. Luo, B. Li, W. Wang, K. Wu, B. Tan, *Adv. Mater.*, 2012, **24**, 5703, (f) P. Hasmukh A, H. Sang, P. Joonho, C. Dennis P, Y. Jung, C T. Yavuz, C. Ali, *Nat. Commun.* 2013, **4***,* 1357; (g) N. Du, H. Park, G. P. Robertson, M. M. Dal-Cin, T. Visser, L. Scoles and M. D. Guiver, *Nat. Mater.,* 2011*,* **10**, 372.

9 (a) M. H. Weston, O. K. Farha, B. G. Hauser, J. T. Hupp, S. T. Nguyen, *Chem. Mater.*, 2012, **24**, 1292; (b) N. B. McKeown, P. M. Budd, Chem. Soc. Rev., 2006, 35, 675; (c) J. X. Jiang, F. Su, A Trewin, C. D. Wood, N. L. Campbell, H. Niu, C. Dickinson, A. Y. Ganin, M. J. Rosseinsky, Y. Z. Khimyak, A. I. Cooper, *Angew. Chem. Int. Ed.*, 2007, **46***,* 8574; (d) R. Dawson, A.I. Cooper, D.J. Adams, *Prog. Polym. Sci*., 2012, **37**, 530; (e)T. Ben, H. Ren, S. Q. Ma, D. P. Cao, J. H. Lan, X. F. Jing, W. C. Wang, J. Xu, F. Deng, J. M. Simmons, S. L. Qiu, G. S. Zhu, *Angew. Chem. Int. Ed.,* 2009, **48***,* 9457; (f)W. Lu, D. Yuan, D. Zhao, C. I. Schilling, O. Plietzsch, T. Muller, S. Bräse, J. Guenther, J. Blümel, R. Krishna, Z. Li, H. C. Zhou, *Chem. Mater.*, 2010, **22***,* 5964; (g) P. Kuhn, M. Antonietti, A. Thomas, *Angew. Chem. Int. Ed.*, 2008, **47***,* 3450; (h) H. Furukawa, O. M. Yaghi, *J. Am. Chem. Soc.*, 2009, **131**, 8875; (i) A. P. Cote, A. I. Benin, N. W. Ockwig, M. O'Keeffe, A. J. Matzger, O. M. Yaghi, *Science*, 2005, **310**, 1166; (j) H. M. Kaderi, J. R. Hunt, J. L. Mendoza, A. P. Cote, R. E. Taylor, M. O'Keeffe, O. M. Yaghi, *Science*, 2007, **316**, 268.

10 (a) W. Lu, J. P. Sculley, D. Yuan, R. Krishna, Z. Wei, H. C. Zhou, *Angew. Chem. Int. Ed.*, 2012, **51**, 7480; (b) R. Dawson, A. Laybourn, Y. Z. Khimyak, D. J. Adams, A. I. Cooper, *Macromolecules*, 2010, **43**, 8524.

11 (a) K. L. Mulfort, O. K. Farha, C. L. Stern, A. A. Sarjeant, J. T. Hupp, *J. Am.Chem. Soc.*, 2009, **131**, 3866; (b) A. Li, R. Lu, Y. Wang, X. Wang, K. Han, W. Deng, *Angew. Chem. Int. Ed.*, 2010, **49**, 3330; (c) K. L. Mulfort, J. T. Hupp, *J. Am.Chem. Soc.*, 2007, **129**, 9604; (d) D. Himsl, D. Wallacher,M. Hartmann, *Angew. Chem. Int. Ed.*, 2009, **48**, 4639; (e) S. Yang, X. Lin, A. J. Blake, K. M. Thomas, P. Hubberstey, N. R. Champness, M. Schröder, *Chem. Commun.*, 2008, 6108; (f) F. Nouar, J. Eckert, J. F. Eubank, P. Forster, M. Eddaoudi, *J. Am. Chem. Soc.*, 2009, **131**, 2864; (h) W. Lu, D. Yuan, J. Sculley, D. Zhao, R. Krishna, H. C. Zhou, *J. Am. Chem. Soc.*, 2011, **133**, 18126; (i) Z. Xiang, Z. Hu, D. Cao, W. Yang, J. Lu, B. Han, W. Wang, *Angew. Chem. Int. Ed.*, 2011, **50**, 491.

12 The palladium-catalyzed Sonogashira-Hagihara cross-coupling reaction is also known for the synthesis of conjugated microporous polymers (CMPs) reported by the group of Andrew I. Cooper. See: (a) J. X. Jiang, F. Su, A. Trewin, C. D. Wood, H. Niu, J. T. A. Jones, Y. Z. Khimyak, A. I. Cooper. *J. Am. Chem. Soc.*, 2008, **130**, 7710; (b) J. X. Jiang, A. Trewin, F. Su, C. D. Wood, H. Niu, J. T. A. Jones, Y. Z. Khimyak, A. I. Cooper, *Macromolecules*, 2009, **42**, 2658; (c) R. Dawson, D. J. Adams, A. I. Cooper, *Chem. Sci.*, 2011, **2,** 1173.

13 E. Stöckel, X. Wu, A. Trewin, C. D. Wood, R. Clowes, N. L. Campbell, J. T. A. Jones, Y. Z. Khimyak, D. J. Adams, A. I. Cooper, *Chem. Commun.*, 2009, 212.

14 R. Dawson, L. A. Stevens, T. C. Drage, C. E. Snape, M. W. Smith, D. J. Adams, A. I. Cooper, *J. Am. Chem. Soc.*, 2012, **134**, 10741.

15 (a) S. K. Bhatia, A. L. Myers, *Langmuir*, 2006, **22**, 1688; (b) R. C. Lochan, M. Head-Gordon, *Phys. Chem. Chem. Phys.*, 2006, **8**, 1357.

16 S. Bourrelly, P. L. Llewellyn, C. Serre, F. Millange, T. Loiseau and G. Ferey, *J. Am. Chem. Soc.*, 2005, **127**, 13519.

17 J. R. Karra and K. S. Walton, *J. Phys. Chem. C*, 2010, **114**, 15735.

18 W. Zhou, H. Wu, M. R. Hartman and T. Yildirim, *J. Phys. Chem. C*, 2007, **111**, 16131.

19 M. G. Rabbani, H. M. El-Kaderi, *Chem. Mater.*, 2012, **24**, 1511.

20 (a) Y.F. He and N.A. Seaton, *Langmuir*, 2005, **21**, 8297;(b) K. Mosher, and W. Jennifer. The Impact of Pore Size On Methane and CO_2 Adsorption In Carbon. Thesis (M.S.)--Stanford University, 2011.
21 A. L. Myers, J. M. Prausnitz, *AIChE J*. 1965, **11**, 121.